Advances in Applied Mathematics and Mechanics
Adv. Appl. Math. Mech., Vol. **9**, No. 6, pp. 1330-1346

DOI: 10.4208/aamm.2016.m1530
December 2017

# Rock Stress Around Noncircular Tunnel: a New Simple Mathematical Method

Wenlong Shen[1,2,*], Xiangyu Wang[2,*], Jianbiao Bai[2], Wenfeng Li[3] and Yang Yu[4]

[1] *School of Energy Science and Engineering, Henan Polytechnic University, Jiaozuo 454000, Henan, China*
[2] *State Key Laboratory of Coal Resources and Mine Safety, China University of Mining & Technology, Xuzhou 221116, Jiangsu, China*
[3] *Mewbourne School of Petroleum and Geological Engineering, University of Oklahoma, Norman, OK 73019, USA*
[4] *School of Civil Engineering; Xuzhou Institute of Technology, Xuzhou 221008, Jiangsu, China*

Received 9 April 2016; Accepted (in revised version) 14 November 2016

**Abstract.** A new simple mathematical method has been proposed to predict rock stress around a noncircular tunnel and the method is calibrated and validated with a numerical model. It can be found that the tunnel shapes and polar angles affect the applicable zone of the theoretical model significantly and the applicable zone of a rectangular tunnel was obtained using this method. The method can be used to predict the values of the concentrated stress, and to analyze the change rate of rock stress and back to calculate the mechanical boundary condition in the applicable zone. The results of the stress change rate indicate that the horizontal stress is negatively related to the vertical boundary load and positively related to the horizontal boundary load. The vertical stress is negatively related to the horizontal boundary load and positively related to the vertical boundary load. These findings can be used to explain the evolution of the vertical increment in stress obtained with field-based borehole stress monitoring.

**AMS subject classifications**: 65M10, 78A48
**Key words**: Rock stress, mathematical model, noncircular tunnel, applicable zone, stress change rate, numerical simulation.

## 1 Introduction

In underground mining operations, openings are generally characterized as having rectangular or other noncircular tunnels. These geometries can result in difficulties and complexities in obtaining and using analytical solutions of rock stress [1, 2]. An analytical

*Corresponding author.
*Email:* wangxiangyu_cumt@163.com (X. Y. Wang), shenwenlong.888@163.com (W. L. Shen)

 ©2017 Global Science Press

https://doi.org/10.4208/aamm.2016.m1530 Published online by Cambridge University Press

solution is often a better and more efficient way to analyze the influence of variables like the boundary conditions on the stress distribution around the tunnel compared with finite element or finite difference numerical methods and can be used to analyze monitored results accurately [3–5]. For example, some analytical solutions for circular tunnel have been obtained around anisotropic materials and widely used combined with some failure criteria [6–11].

The precious complex variable theory and conformal mapping method is widely used to solve the analytical solution of stress around a noncircular tunnel in underground engineering [12–15]. Using this method, Huo et al. [16] deduced an analytical solution and revealed the effect of the far-field shear stress on the stability of a rectangular structure around the rectangle tunnel. Combining with the power series method, the analytical solution of the stress around an arbitrary shaped tunnel section was obtained and the results agree well with that from the numerical simulation model [17]. By introducing a general form of mapping function and an arbitrary biaxial loading into the boundary conditions, the general analytical solution of the stress around the arbitrary shaped tunnel was successfully revealed and used [18].

A new simple method, referred to as "equivalent radius", first put forward by Liu et al. [19] has become widely used in engineering analyses in China [20–22]. The applicability and the reasonability of this method for noncircular tunnels have not been adequately investigated. Therefore, using a rectangular tunnel, we assessed the new method for obtaining an equivalent radius for the theoretical model. We successfully solved the following problems: the establishment and verification of a theoretical model, the definition of an acceptable zone around the rectangle tunnel in which the new and original methods could be applied, and the application of a theoretical model for analyzing the stress change rate induced by the boundary load and in predicting the concentrated stress within the acceptable zone.

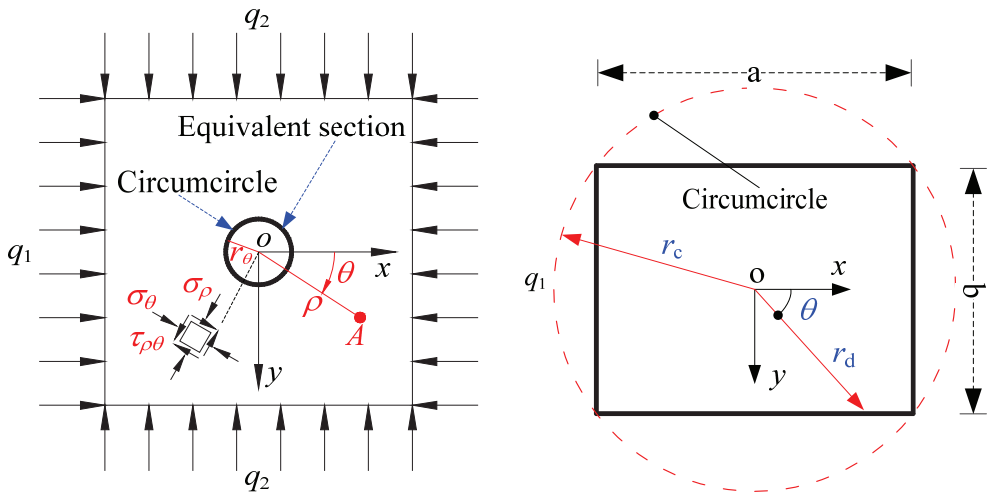
## 2 Method introduction

### 2.1 Theoretical model

Four elements: burial depth, lithology, boundary conditions and section shape, were considered to establish the theoretical model (Fig. 1). The sectional area of an underground opening is generally very small compared with the burial depth. In order to keep the model as simple as possible, the boundary conditions assumed pertaining to a uniformly distributed load ($q_1$ and $q_2$ in Fig. 1). Regardless of whether the rock being examined is igneous, sedimentary or metamorphic, it can be either isotropic or anisotropic. Here, we simply assume that the lithology around the openings is isotropic and homogeneous. Furthermore, we use the equivalent radius instead of a noncircular section shape like a rectangle.

The following values were established to calculate the stress around the noncircular openings: a circumcircle radius ($r_c$), a constant representing the distance ($r_d$) between

https://doi.org/10.4208/aamm.2016.m1530 Published online by Cambridge University Press




(a) Mechanical model (b) Mathematical model

Figure 1: Theoretical model for equivalent radius.

the surface and the center of the section, and a variable value for the equivalent radius. The rectangular section presented as Eq. (2.1b) and Fig. 1(b) shows that $r_d$ is a function of $\theta$. The first quadrant ($0^\circ \le \theta \le 90^\circ$) can be considered independently because the rectangular section has a central symmetry. An analytical solution for the stress around the circumcircle section can be determined as shown in Eq. (2.1c) [23]. The analytical solution for the rectangular coordinate system is presented in Eq. (2.1d) according to coordinate transformation [23]. So the analytical solution for the stress around circular tunnel can be used to predict the stress around the noncircular tunnel by means of equivalent radius as shown in Fig. 1(b). However, the applicability for the method needs to be verified:

$$r_\theta = r_c = \frac{\sqrt{a^2+b^2}}{2}, \tag{2.1a}$$

$$r_\theta = r_d = \begin{cases} \dfrac{a}{2\cos\theta}, & 0 \le \theta < \arctan\dfrac{b}{a}, \\ \dfrac{b}{2\sin\theta}, & \arctan\dfrac{b}{a} \le \theta \le 90, \end{cases} \tag{2.1b}$$

$$\begin{cases} \sigma_\rho = \dfrac{q_1+q_2}{2}\left(1-\dfrac{r_\theta^2}{\rho^2}\right) + \dfrac{q_1-q_2}{2}\left(1-\dfrac{r_\theta^2}{\rho^2}\right)\left(1-3\dfrac{r_\theta^2}{\rho^2}\right)\cos 2\theta, \\ \sigma_\theta = \dfrac{q_1+q_2}{2}\left(1+\dfrac{r_\theta^2}{\rho^2}\right) - \dfrac{q_1-q_2}{2}\left(1+3\dfrac{r_\theta^4}{\rho^4}\right)\cos 2\theta, \\ \tau_{\rho\theta} = \dfrac{q_2-q_1}{2}\left(1-\dfrac{r_\theta^2}{\rho^2}\right)\left(1+3\dfrac{r_\theta^2}{\rho^2}\right)\sin 2\theta, \end{cases} \tag{2.1c}$$

https://doi.org/10.4208/aamm.2016.m1530 Published online by Cambridge University Press

$$\begin{cases} \sigma_x = \dfrac{\sigma_\rho + \sigma_\theta}{2} + \dfrac{\sigma_\rho - \sigma_\theta}{2}\cos 2\theta - \tau_{\rho\theta}\sin 2\theta, \\ \sigma_y = \dfrac{\sigma_\rho + \sigma_\theta}{2} - \dfrac{\sigma_\rho - \sigma_\theta}{2}\cos 2\theta + \tau_{\rho\theta}\sin 2\theta. \end{cases} \tag{2.1d}$$

## 2.2 Numerical simulation verification

Theoretical models of underground openings need to be confirmed as being applicable to The actual situations. Elastic models were used to calculate the stress around the openings, before the openings are excavated, the boundary conditions, as well as the stress states, in the numerical model must be consistent with those of the theoretical model (as shown in Fig. 1(a)). Thus, the process of the numerical calculation was divided into three steps. The global model was generated with reasonable mesh in the first step. In the second step, the geostatic stress condition was applied. In the third step, the tunnel was developed and solving until in the state of equilibrium. When the boundary condition and tunnel dimension vary, the process of numerical calculation can repeat.

The model was established in FLAC3D with dimensions of $100\times20\times100$m (along the $x$, $y$ and $z$ axes, respectively) as shown in Fig. 2. It is composed of two parts: inner model with radcylinder mesh (inner model with radtunnel mesh for rectangle tunnel) and outer model with radtunnel mesh, that enable all individual zones around the tunnel to be small enough. The radial cylinder model has dimensions of $40\times20\times40$m. The surrounding radial tunnel model has dimension of $100\times20\times100$m. We selected realistic values for the bulk modulus (2GPa) and shear modulus (also 2GPa) as parameters in the simulation model. The vertical stress was determined using the gravitational load, whereas the horizontal stress was determined by combining the vertical stress with a lateral pressure coefficient of 1.2. The upper and lower boundaries were applied with a vertical stress of $q_2$ (Here $q_2$ equals $-10$MPa.). Side boundaries were applied with a

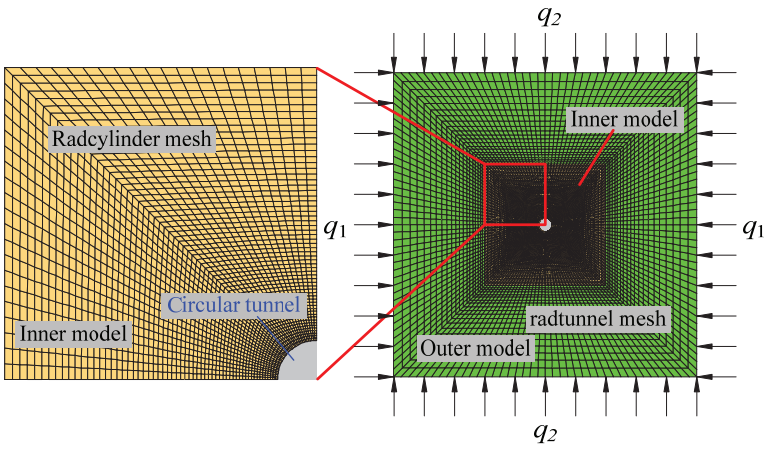



Figure 2: Numerical simulation model.

https://doi.org/10.4208/aamm.2016.m1530 Published online by Cambridge University Press

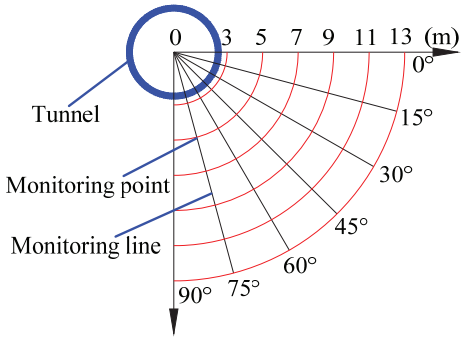



Figure 3: Monitoring point distribution.

horizontal stress of $q_1$ (Here $q_1$ equals $-12$MPa). The front and back boundaries were fixed with displacement in the normal direction. Individual zones within the simulation model were initialized with a vertical stress of $q_2$ and a horizontal stress of $q_1$.

Monitoring points (42 in total) were arranged in the model section ($y$=10m) (as shown in Fig. 3). They recorded the stress variation every tenth step until the individual zone reached a state of equilibrium. Then, the last data recorded were compared with the theoretical conclusions (Fig. 4).

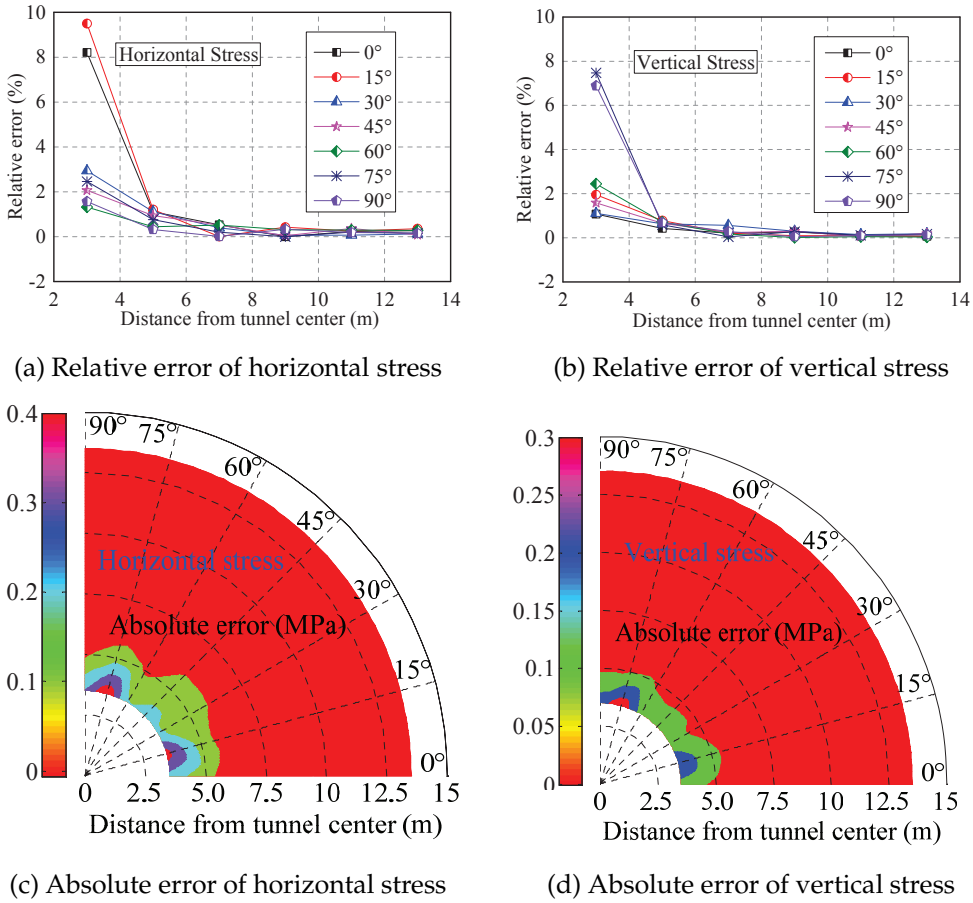
The theoretical results agree well with the simulations for vertical and horizontal stress associated with a circular tunnel; the absolute error between them is within 0.5MPa (Figs. 4(c), (d)). The absolute error decreases sharply between distances of 3 and 5m and then decreases fairly slowly as the distance increases from 5 to 10m. The polar angle greatly influences the absolute error in shallow rock but has little influence on the absolute error in deep rock. The relative error (Figs. 4(a), (b)) is less than 3%, except for polar angles of 0° to 15° for the horizontal stress and 75° to 90° for the vertical stress in shallow rock. Succinctly, the theoretical results for a circular tunnel can be compared acceptably with simulations, with absolute and relative errors less than 0.5MPa and 10%, respectively.

# 3 Application and results for rectangular tunnel

## 3.1 Acceptable zone

The polar angle greatly influences the absolute error between theoretical results and simulations for a rectangular tunnel (Figs. 5(c), (d)). For horizontal stress, the absolute error will be $<$1MPa when the polar angle lies between 60° and 90°, regardless of the distance from the tunnel center. It will be $>$1MPa, and possibly as high as 5MPa, when the polar angle lies between 0° and 45° in shallow rock (approximately 5 to 7m from the tunnel center, depending on the polar angle) around the tunnel. In addition, it will be $<$1MPa and will decrease fairly slowly in deep rock around the tunnel. For the vertical stress, the

https://doi.org/10.4208/aamm.2016.m1530 Published online by Cambridge University Press




(a) Relative error of horizontal stress

(b) Relative error of vertical stress

(c) Absolute error of horizontal stress

(d) Absolute error of vertical stress

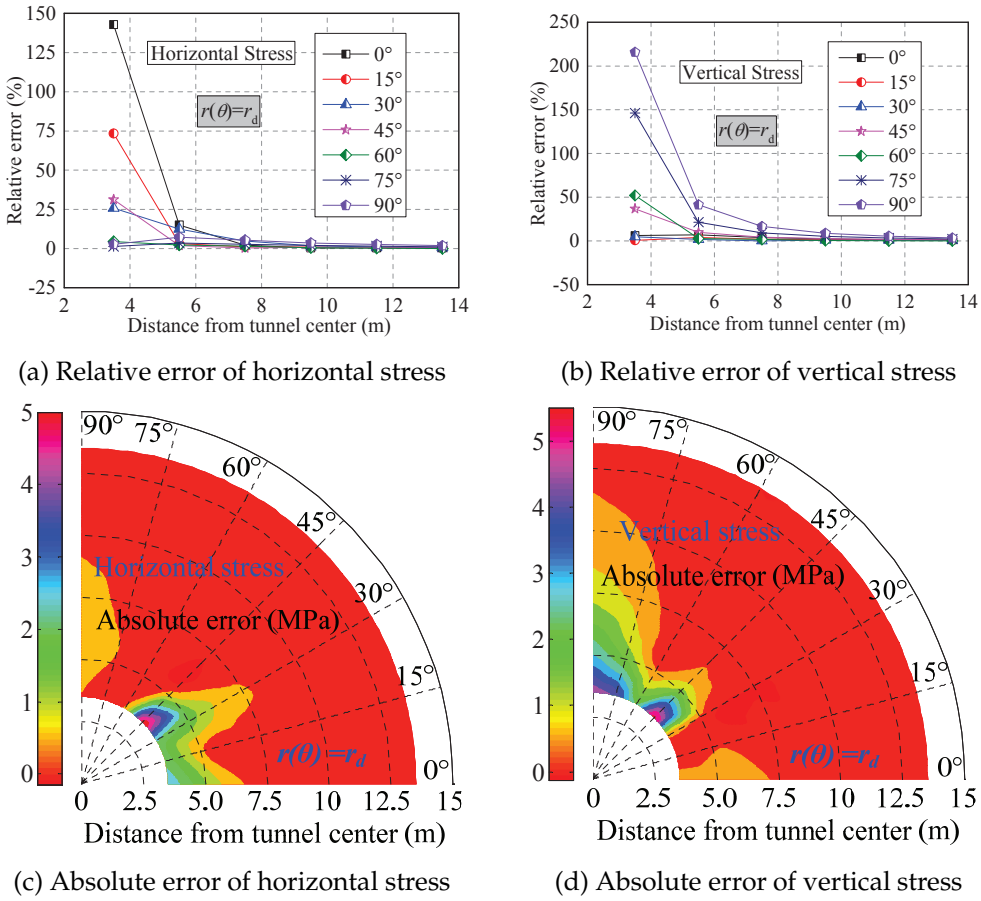
Figure 4: Comparison with numerical calculations for a circular tunnel.

absolute error will be $<$1MPa when the polar angle lies between 0° and 30°, regardless of the distance from the tunnel center. It will be $>$1MPa, and again as high as 5MPa, when the polar angle lies between 45° and 90° in shallow rock around the tunnel. Similar to the horizontal stress, the vertical stress will be $<$1MPa and will decrease fairly slowly in deep rock around the tunnel.

The relative error is $<$7.3% for the horizontal stress (Fig. 4(a)) when the polar angle lies between 60° and 90°, whereas it exceeds 25% (and can reach even 142%) when the polar angle lies between 0° and 45° in shallow rock. In contrast, it is $<$6.8% for vertical stress (Fig. 5(b)) when the polar angle lies between 0° and 30°, whereas it exceeds 36% (even reaching 215%) when the polar angle lies between 45° and 90° in shallow rock.

Compared with the results obtained with Eq. (2.1b), the relative and absolute error as shown in Figs. 6(a)-(d) obtained with Eq. (2.1a) were almost identical to those from a deep rock setting, but quite different to those from shallow rock. For example, when the

https://doi.org/10.4208/aamm.2016.m1530 Published online by Cambridge University Press




(a) Relative error of horizontal stress

(b) Relative error of vertical stress

(c) Absolute error of horizontal stress

(d) Absolute error of vertical stress

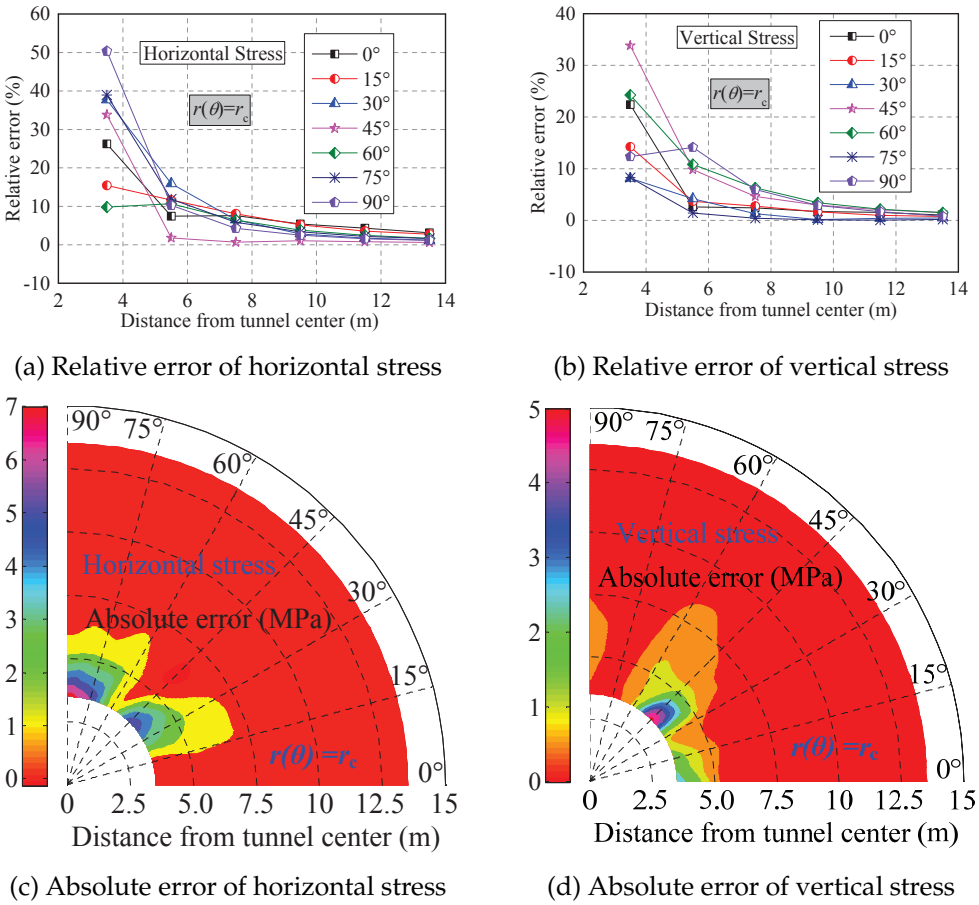
Figure 5: Comparison with numerical calculations for $r_d$ in a rectangular tunnel.

polar angle equals 0° and 15°, the absolute error of the horizontal stress is $<$1MPa, with a relative errors of 26.23% and 15.45%, respectively in shallow rock; when the polar angle equals 75° and 90°, the absolute error of the vertical stress is $<$1MPa, with relative errors of 8.27% and 12.35%, respectively in shallow rock.

## 3.2 Prediction of high stress concentration

Based on the analysis above, there is an acceptable zone around the rectangular tunnel for the theoretical model using Eq. (2.1b), i.e., 60° to 90° in shallow rock and 0° to 90° in deep rock for horizontal stresses, and 0° to 30° in shallow rock and 0° to 90° in deep rock for vertical stresses (Fig. 7). This presents a similar distribution, with the concentration factor in the shallow rock around a tunnel as shown in Fig. 8. The acceptable zone in shallow rock is located within the high stress zone, whereas the unacceptable zone in the shallow rock is located within the low stress zone for both horizontal and vertical stresses.

https://doi.org/10.4208/aamm.2016.m1530 Published online by Cambridge University Press




(a) Relative error of horizontal stress

(b) Relative error of vertical stress

(c) Absolute error of horizontal stress

(d) Absolute error of vertical stress

Figure 6: Comparison with numerical calculation for $r_c$ in a rectangular tunnel.

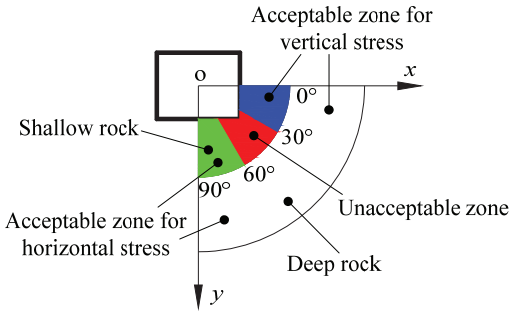
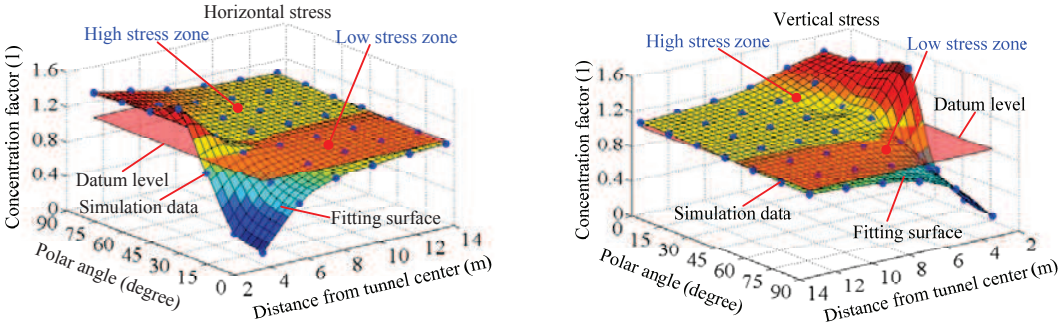



Figure 7: Applicable zone for vertical and horizontal stresses in the theoretical model.

These findings can readily be applied to predict high stress values in some zones around a rectangular tunnel.

https://doi.org/10.4208/aamm.2016.m1530 Published online by Cambridge University Press




(a) Horizontal stress (b) Vertical stress

Figure 8: Stress concentration factor around tunnel.

### 3.3 Change rate induced from mechanical boundary conditions

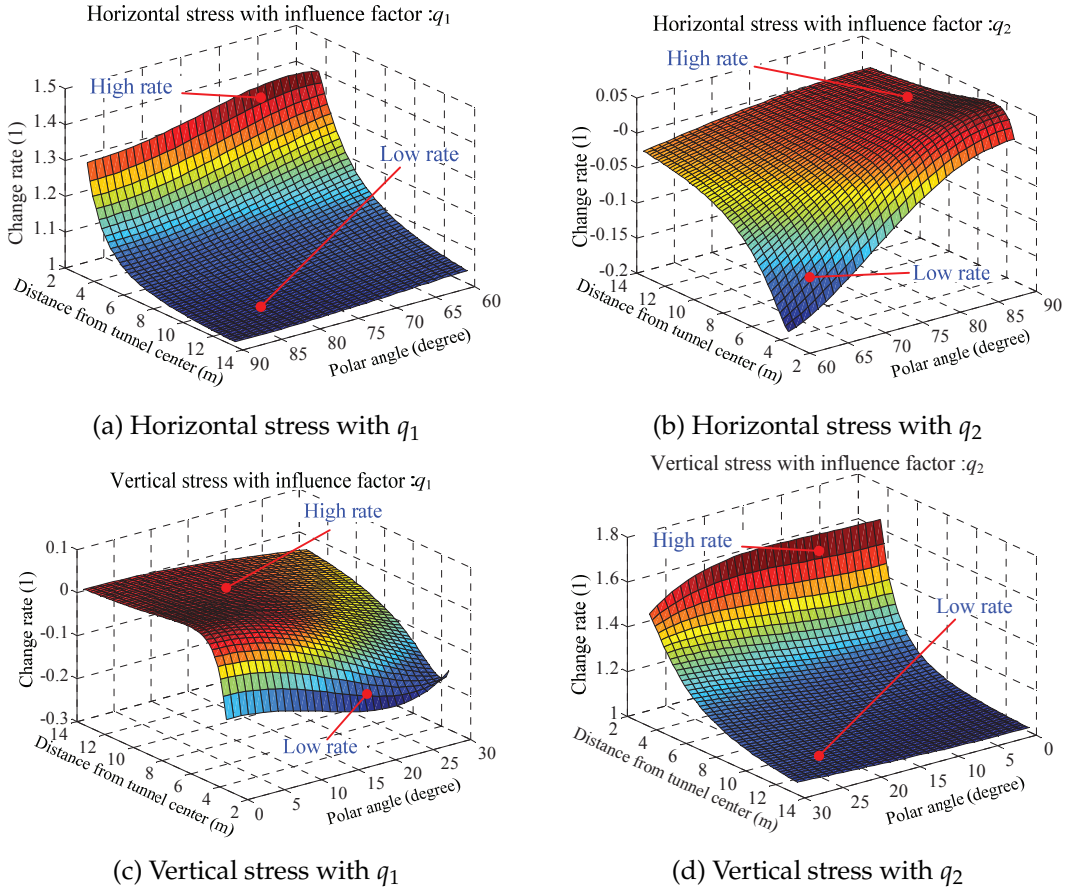
In the vicinity of a tunnel, both vertical and horizontal stresses will change as the boundary conditions vary; this is especially so for the mechanical boundary. With the partial differential principle applied to the theoretical model, the change rates of vertical and horizontal stresses for any acceptable point around a rectangular tunnel can be determined by Eq. (3.1) and Fig. 9. The horizontal stress interestingly is found to increase as the horizontal load $q_1$ increases (Fig. 9(a)) and decrease as the vertical load $q_2$ increases (Fig. 9(b)). However, vertical stress will decrease with an increase in horizontal load $q_1$ (Fig. 9(c)) and will increase with an increase in vertical load $q_2$ (Fig. 9(d)). In addition, the change rate for the stress is different when the point location varies. As an example, Fig. 9(a) shows that the change rate of the horizontal stress induced with $q_1$ decreases slowly as the polar angle increases, but increases following an index law as the distance from the tunnel center decreases. This means that distance is the main influence on the change rate

$$\begin{cases} \dfrac{\partial\sigma_x}{\partial q_1}=1+\dfrac{r_\theta^2}{\rho^2}-\dfrac{3r_\theta^4}{2\rho^4}-\dfrac{3r_\theta^2}{2\rho^2}\cos 2\theta+\left(\dfrac{3r_\theta^4}{\rho^4}-\dfrac{2r_\theta^2}{\rho^2}\right)\cos^2 2\theta, \\ \dfrac{\partial\sigma_x}{\partial q_2}=-\dfrac{r_\theta^2}{\rho^2}+\dfrac{3r_\theta^4}{2\rho^4}+\dfrac{r_\theta^2}{2\rho^2}\cos 2\theta-\left(\dfrac{3r_\theta^4}{\rho^4}-\dfrac{2r_\theta^2}{\rho^2}\right)\cos^2 2\theta, \\ \dfrac{\partial\sigma_y}{\partial q_1}=-\dfrac{r_\theta^2}{\rho^2}+\dfrac{3r_\theta^4}{2\rho^4}-\dfrac{r_\theta^2}{2\rho^2}\cos 2\theta-\left(\dfrac{3r_\theta^4}{\rho^4}-\dfrac{2r_\theta^2}{\rho^2}\right)\cos^2 2\theta, \\ \dfrac{\partial\sigma_y}{\partial q_2}=1+\dfrac{r_\theta^2}{\rho^2}-\dfrac{3r_\theta^4}{2\rho^4}+\dfrac{3r_\theta^2}{2\rho^2}\cos 2\theta+\left(\dfrac{3r_\theta^4}{\rho^4}-\dfrac{2r_\theta^2}{\rho^2}\right)\cos^2 2\theta. \end{cases} \tag{3.1}$$

### 3.4 Case analysis

The example in Fig. 9 could benefit the stress monitoring and analysis for a specific case in the acceptable zone. In underground mining excavations [24–26], many types of open-

https://doi.org/10.4208/aamm.2016.m1530 Published online by Cambridge University Press




(a) Horizontal stress with $q_1$

(b) Horizontal stress with $q_2$

(c) Vertical stress with $q_1$

(d) Vertical stress with $q_2$

Figure 9: Stress change rate around a tunnel.

ings will encounter significant deformation, roof fall, rock burst or other dynamic disasters due to the fact that the boundary loads around the space are in a variable state, including engineering conditions and unpredictable geological settings. The following case is referred to the mining engineering condition which can be seen as the mechanical boundary conditions. From the analysis process, an interesting and efficient method to design the tunnel is founded. First, the stress can be monitored with different polar angle and polar radius in the acceptable zone around the tunnel. Second, with the change rate considered (like Fig. 9), the key influence factor can be obtained ($q_1$ or $q_2$). Third, according to Eq. (2.1c) and Fig. 7 the mechanical boundary condition including $q_1$ or $q_2$ can be obtained by back calculation. At last we can use the real mechanical boundary condition to design the tunnel.

Change rates can be used to analyze the following engineering case from Majialiang coal mine in China (Fig. 11(a)), in which the entry heading runs adjacent to the working face [27]. Majialiang coal mine is similar to the Xichuan coal mine [27] in terms of engi-

https://doi.org/10.4208/aamm.2016.m1530 Published online by Cambridge University Press

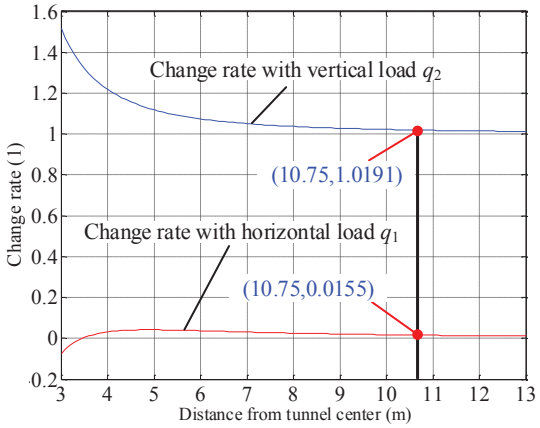
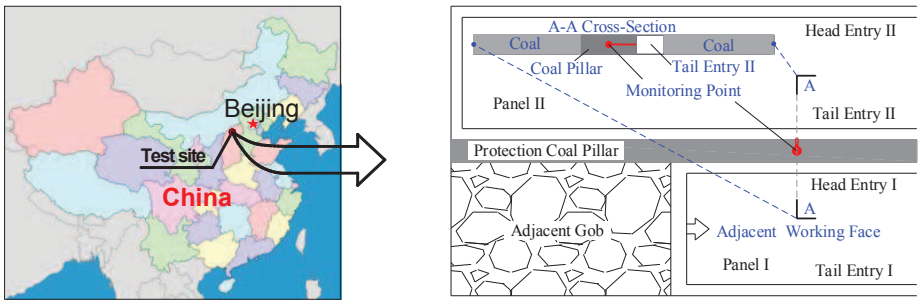



Figure 10: Change rate with polar angle 180°.




(a) Mine location (b) Longwall panels layout

Figure 11: Mine location and panels layout of the test site.

neering conditions, but not in terms of geological conditions. The mine is located near the city of Shuozhou, Shanxi Province, China. Consider the mine's coal seam 4, which has an average thickness, burial depth, and dip angle of 9.78m, 640m, and 2°, respectively. The immediate roof is a 0.5-m-thick kaolin mudstone with uniaxial compressive strength of 51.7MPa, classified as a medium hard rock. The basic roof above that consists of a 0.81-m-thick medium sandstone, a 1.17-m-thick grit sandstone, and a 5.51-m-thick fine sandstone with uniaxial compressive strengths of 74.4, 84.8, and 82.8MPa, respectively, classified as hard rocks. The immediate floor is a 1.16m-thick carbonaceous mudstone with a uniaxial compressive strength of 32.1MPa, classified as a soft rock. The basic floor below that consists of a 3.00m-thick medium sandstone and a 0.98m-thick fine sandstone with uniaxial compressive strengths of 66.0 and 69.2MPa, respectively, classified as medium hard rocks. In addition, the rectangular entry is $5.5\times4.0$m in size, with 20m-wide protection coal pillars.

https://doi.org/10.4208/aamm.2016.m1530 Published online by Cambridge University Press

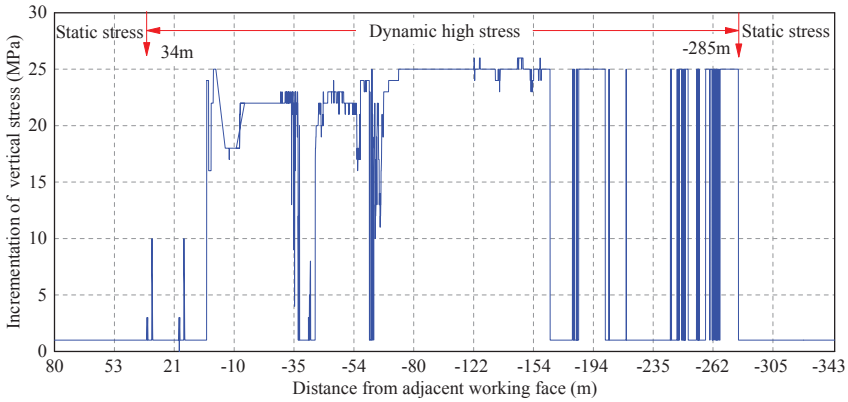



Figure 12: Increments of vertical stress around the tunnel.

The change rate in evolution (Fig. 10) calculated in Eq. (3.1) is identical to that in polar angle 0° because the monitoring point is located in a rib with a polar angle of 180°. The change rate for vertical load $q_2$ is found to decrease following an index law as the distance from the tunnel center increases. In contrast, for a horizontal load, $q_1$ will increase first and then decrease with increasing distance. The change rate for vertical stress is greatly influenced by the vertical load $q_2$ but is little influenced by the horizontal load $q_1$ due to the fact that the change rate is 1.0191 (slightly more than unity) and 0.0155 (approximately zero). Therefore, we can back calculate the vertical load $q_2$, approximately, with the monitoring vertical stress.

Fig. 12 illustrates the evolution of the vertical stress as it increments at the monitoring point in the entry rib with a polar angle of 180° as shown in Fig. 11(b) during the period over which the adjacent working face advanced. The monitoring instrument was in its normal working state at the front of the adjacent working face (finishing 80m behind the adjacent working face at a distance of 343m). It is obvious that the vertical stress increment can be divided into three stages: static stress in the front of the adjacent working face, high dynamic stress, and static stress behind of the adjacent working face induced as "$q_1$ in stage I", "$q_2(r)$ and $q_3\max(s)$ in stage II", and "$q_4(t)$ in stage III", respectively, based on Bai et al. [27]. So with the method of back calculation, the practical stress condition will be obtained rather than the numerical simulation.

As discussed above, the vertical load $q_2$ for this case will evolve in the following process. The region of high dynamic stress extends from 34m in front of an advancing working face to 285m behind it. The front abutment stress is characterized by its short-lived nature, lower-frequency, and approximately 10MPa peak increment between 34 and 15m of the advancing working face. However, the lateral abutment stress behind the adjacent working face is characterized by a long-term, high-frequency, state of undulation between 15 and 25MPa, with the peak increment extending to 285m behind the advancing working face.

https://doi.org/10.4208/aamm.2016.m1530 Published online by Cambridge University Press

# 4 Discussion

Compared with previous methods [19], this theoretical model is more realistic because the equivalent radius, the distance between the center of the tunnel and the surface, is a function of polar angle rather than the circumcircle radius with the shallow rock ignored. Additionally, the results for a rectangular tunnel indicate that the method used to obtain an equivalent radius for Eq. (2.1a) and Eq. (2.1b) is applicable to different polar angles. Therefore, they can be used together to expand the range of applications possible with this theoretical model.

However, whether the theoretical model is acceptable or not when the dimension of the tunnel and the mechanical boundary conditions vary. With a same analysis procedure in Section 3.1, the acceptable zone for different schemes (Table 1) is presented in Fig. 13 and Fig. 14. The criteria for the division is that it is considered as acceptable zone where the absolute error is less than 1MPa and the relative error is less than 10%. Obviously, they present a similar distribution for the acceptable zone and the unacceptable zone for the theoretical model. However, there are some differences between them. For example, as the mechanical boundary condition varies form scheme A to scheme C (Fig. 13), the unacceptable zone extends mainly along the tunnel radial direction to the depth rather than the circumferential direction. Varying from scheme D to scheme F, dimension of the rectangle tunnel is identical with the mechanical boundary condition in the extension of the unacceptable zone. But the shape of the unacceptable zone will change when the dimension of the tunnel vary (Fig. 14).

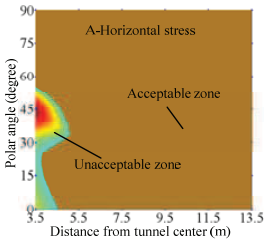
An interesting result is that the change rate in stress in the zone around a tunnel is a linear function of the boundary load $q_1$ and $q_2$. The horizontal stress around the tunnel is negatively related to the vertical load $q_2$, the secondary factor of influence, and positively related to the horizontal load $q_1$, the decisive factor. However, the vertical stress around the tunnel is inversely related to the horizontal load $q_1$, the secondary influencing factor, and directly related to the vertical load $q_2$, the decisive factor. As the evolution of vertical stress increments in the rib of the entry driving ahead of the advancing working face, as analyzed based on the above findings, the vertical load $q_2$ induced by movement in the overburden strata will evolve in a similar way.

Note that there are some assignments to make with the theoretical model. First, the analytical solution for rock stress around a noncircular tunnel can be used only in an elastic region. Therefore, we aim to optimize the equivalent radius function. For example, the

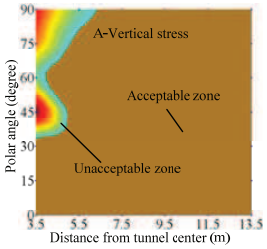
Table 1: Numerical simulation schemes for the verification of theoretical model.

| Mechanical boundary conditions | | | Dimension of the rectangle tunnel | | |
|---|---|---|---|---|---|
| A | B | C | D | E | F |
| $q_1=-6$MPa<br>$q_2=-5$MPa | $q_1=-12$MPa<br>$q_2=-10$MPa | $q_1=-18$MPa<br>$q_2=-15$MPa | 4m×4m | 5m×4m | 6m×4m |
| Dimension: 5m×4m (width×height) | | | $q_1=-12$MPa and $q_2=-10$MPa | | |

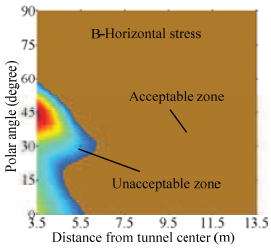
https://doi.org/10.4208/aamm.2016.m1530 Published online by Cambridge University Press



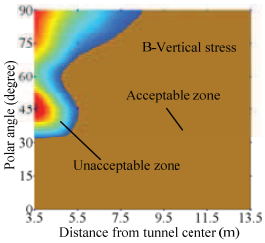

(a) Scheme A for horizontal stress



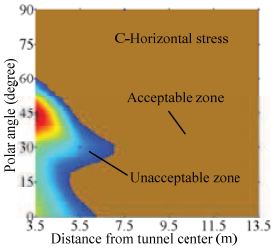

(b) Scheme A for vertical stress



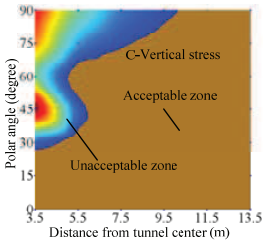

(c) Scheme B for horizontal stress




(d) Scheme B for vertical stress

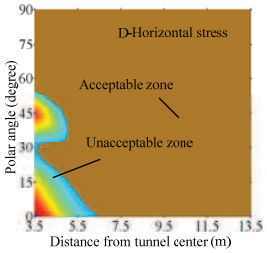



(e) Scheme C for horizontal stress

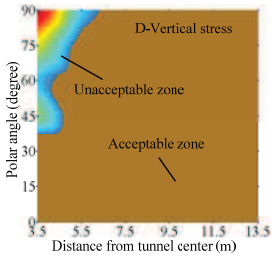



(f) Scheme C for vertical stress

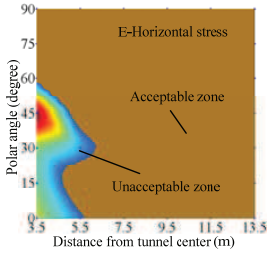
Figure 13: Relationship between acceptable zone and mechanical boundary condition.



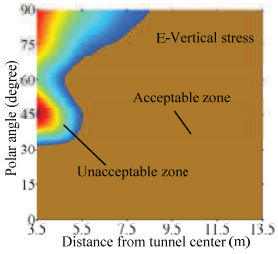

(a) Scheme D for horizontal stress



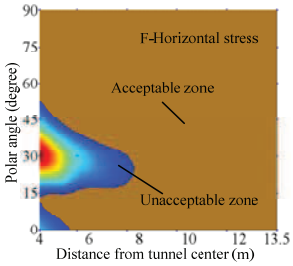

(b) Scheme D for vertical stress



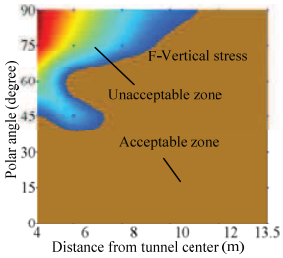

(c) Scheme E for horizontal stress




(d) Scheme E for vertical stress




(e) Scheme F for horizontal stress




(f) Scheme F for vertical stress

Figure 14: Relationship between acceptable zone and dimension of the rectangle tunnel.

https://doi.org/10.4208/aamm.2016.m1530 Published online by Cambridge University Press

equivalent radius can be imagined as a function of the distance from the tunnel center to the elastic-plastic interface. Second, this method may be improved in the range of application around the noncircular tunnel taken in consideration with the stress concentration at the corners of the section or in zones of high curvature.

## 5 Conclusions

The method presented here provides a better way to establish a practical and simple theoretical model using the method of equivalent radius for solving rock stress around a noncircular tunnel. Compared with numerical simulations, the theoretical model can generally be applied to an area referred to as the applicable zone. Over these applicable zone, the method can approximately predict high stress values, analyze the change rate of the rock stress and back calculate the practical mechanical boundary condition with borehole stress monitoring of the tunnel in the field.

Changes in the rate of horizontal and vertical stress on the boundary load are a function of polar angle and distance from the tunnel center in the applicable zone and the distance is the main factor of influence on the change rate. The horizontal stress around the tunnel is inversely related to the vertical boundary load and is directly related to the horizontal boundary load. Similarly, the vertical stress around the tunnel is inversely related to the horizontal boundary load and is directly related to the vertical boundary load.

## Acknowledgments

This work is supported by the National Natural Science Foundation of China through contracts Nos. 51474209, 51574227 and 51604268, the Fundamental Research Funds for the Central Universities (No. 2014XT01), the Project Funded by the Priority Academic Program Development of Jiangsu Higher Education Institutions (No. SZBF2011-6-B35), the Research Innovation Program for College Graduates of Jiangsu Province (No. KYLX16_0559).

## References

[1] G. HASAN, *An elastic solution for stresses around tunnels with conventional shapes,* Int. J. Mining Sci. Tech., 34 (1997).

[2] P. P. HUANGFU, L. Q. ZHANG AND F. Q. WU, *Research on analytical solution of stress field of surrounding rock of single hole with arbitrary shape based on highly-efficient conformal mapping,* Chinese J. Rock Mech. Eng., S2 (2011), pp. 3905–3913.

[3] C. CARRANZA-TORRES AND C. FAIRHURST, *The elasto-plastic response of underground excavations in rock masses that satisfy the Hoek-Brown failure criterion,* Int. J. Rock Mech. Mining Sci., 36 (1999), pp. 777–809.

https://doi.org/10.4208/aamm.2016.m1530 Published online by Cambridge University Press

[4] M. R. ISLAM AND R. SHINJO, *Numerical simulation of stress distributions and displacements around an entry roadway with igneous intrusion and potential sources of seam gas emission of the Barapukuria coal mine, NW Bangladesh,* Int. J. Coal Geology, 78 (2009), pp. 249–262.
[5] N. HOSSEINI, K. ORAEE, K. SHAHRIAR AND K. GOSHTASBI, *Studying the stress redistribution around the longwall mining panel using passive seismic velocity tomography and geostatistical estimation,* Arabian J. Geosci., 6 (2011), pp. 1407–1416.
[6] A. M. HEFNY AND K. Y. LO, *Analytical solution for stresses and displacements around tunnels driven in cross-anisotropic rocks,* Int. J. Numer. Anal. Methods Geomech., 23 (1999), pp. 161–177.
[7] K. M. LEE, X. Y. HOU, X. W. GE AND Y. TANG, *An analytical solution for a jointed shield-driven tunnel lining*, Int. J. Numer. Anal. Methods Geomech., 25 (2001), pp. 365–390.
[8] Y.-E. LU AND W. YANG, *Analytical solutions of stress and displacement in strain softening rock mass around a newly formed cavity,* J. Central South University, 20 (2013), pp. 1397–1404.
[9] N. I. MUSKHELISHVILI, *Some basic problems of the mathematical theory of elasticity,* Mathematical Gazette, 48 (1964), pp. 445–447.
[10] K.-H. PARK AND Y.-J. KIM, *Analytical solution for a circular opening in an elastic-brittle-plastic rock,* Int. J. Rock Mech. Mining Sci., 43 (2006), pp. 616–622.
[11] S. K. SHARAN, *Analytical solutions for stresses and displacements around a circular opening in a generalized Hoek-Brown rock,* Int. J. Rock Mech. Mining Sci., 45 (2008), pp. 78–85.
[12] Q. FENG, B.-S. JIANG, Q. ZHANG AND L. P. WANG, *Analytical elasto-plastic solution for stress and deformation of surrounding rock in cold region tunnels,* Cold Regions Sci. Tech., 108 (2014), pp. 59–68.
[13] K.-H. HAN, C.-P. ZHANG AND M.-S. WANG, *Explicit analytical solutions for stress and displacement of surrounding rock in shallow tunnels,* Chinese J. Geotechnical Eng., 36 (2014), pp. 2253–2259.
[14] A. R. KARGAR, R. RAHMANNEJAD AND M. A. HAJABASI, *A semi-analytical elastic solution for stress field of lined non-circular tunnels at great depth using complex variable method,* Int. J. Solids Struct., 51 (2014), pp. 1475–1482.
[15] A. VRAKAS AND G. ANAGNOSTOU, *A finite strain closed-form solution for the elastoplastic ground response curve in tunnelling,* Int. J. Numer. Anal. Methods Geomech., 38 (2014), pp. 1131–1148.
[16] H. HUO, A. BOBET, G. FERNÁNDEZ AND J. RAMÍREZ, *Analytical solution for deep rectangular structures subjected to far-field shear stresses,* Tunnelling and Underground Space Technology, 21 (2006), pp. 613–625.
[17] A. Z. LU, N. ZHANG, X. L. ZHANG, D. H. LU AND W. S. LI, *Analytic method of stress analysis for an orthotropic rock mass with an arbitrary-shaped tunnel,* Int. J. Geomech., 15 (2015).
[18] V. G. UKADGAONKER AND D. K. N. RAO, *A general solution for stresses around holes in symmetric laminates under inplane loading*, Compos. Struct., 49 (2000), pp. 339–354.
[19] C.-W. LIU, L. CAO AND S.-X. LIU, *Method of equivalent radius for the analyzing rock stress of high-buried non-circular underground chambers,* Chinese J. Copper Eng., (2010), pp. 1–5.
[20] W.-L. SHEN, J.-B. BAI, Y. YU, F. LIU AND Z.-F. HUANG, *Research on floor heave mechanism and control technology of muddy floor roadway under dynamic pressure,* Chinese J. Coal Sci. Tech., 42 (2014), pp. 28–31.
[21] Y. YU, J. BAI, X. WANG, W. SHEN AND C. LIAN, *Study on asymmetric distortion and failure characteristics and stability control of soft rock roadway,* J. Mining Safety Eng., 31 (2014), pp. 340–346.
[22] W.-H. ZHA, X.-Z. HUA AND D.-H. CHEN, *Quantitative Analysis of plastic region in deep buried*

https://doi.org/10.4208/aamm.2016.m1530 Published online by Cambridge University Press

*tunnel based on in-situ stress test,* Chinese J. Experimental Mech., 28 (2013), pp. 657–662.
[23] Z.-L. XU, Elasticity, 4th ed. Beijing, China, Higher Education Press, (2006), pp. 73–77.
[24] M. SHABANIMASHCOOL AND C. C. LI, *Numerical modelling of longwall mining and stability analysis of the gates in a coal mine,* Int.J. Rock Mech. Mining Sci., 51 (2012), pp. 24–34.
[25] S. YAN, J. BAI, X. WANG AND L. HUO, *An innovative approach for gateroad layout in highly gassy longwall top coal caving,* Int. J. Rock Mech. Mining Sci., 59 (2013), pp. 33–41.
[26] W. L. SHEN, J. B. BAI, X. Y. WANG AND Y. YU, *Response and control technology for entry loaded by mining abutment stress of a thick hard roof,* Int. J. Rock Mech. Mining Sci., 90 (2016), pp. 26–34.
[27] J. B. BAI, W. L. SHEN, G. L. GUO, X. Y. WANG AND Y. YU, *Roof deformation, failure characteristics, and preventive techniques of gob-side entry driving heading adjacent to the advancing working face,* Rock Mech. Rock Eng., 48 (2015), pp. 2447–2458.

https://doi.org/10.4208/aamm.2016.m1530 Published online by Cambridge University Press